Energy Conversion and Management 298 (2023) 117812

Contents lists available at ScienceDirect

Energy Conversion and Management

journal homepage: www.elsevier.com/locate/enconman

Comprehensive process simulation of a biomass-based hydrogen production system through gasification within the BECCS concept in a commercial two-stage fixed bed gasifier

Karim Rabea [a,b,*], Stavros Michailos [c], Kevin J. Hughes [a], Derek Ingham [a], Mohamed Pourkashanian [a]

[a] Energy 2050, Translational Energy Research Centre (TERC), Department of Mechanical Engineering, Faculty of Engineering, University of Sheffield, United Kingdom
[b] Mechanical Power Engineering Department, Faculty of Engineering, Tanta University, Tanta 31511, Egypt
[c] School of Engineering, University of Hull, Hull HU6 7RX, United Kingdom

ARTICLE INFO

Keywords:
Hydrogen
Two-stage gasifier
Kinetic model
BECCS
Oxy-steam gasification
Negative emissions

ABSTRACT

Hydrogen production through biomass gasification coupled with carbon capture has the potential to be a net negative emission process. Among the different designs of biomass gasifiers, the two-stage fixed bed gasifier has proved its ability to produce high quality syngas with minimum tar content at an industrial scale. However, it has not been investigated for hydrogen production. Hence, the current study is the first attempt to assess, through process modelling, the technical feasibility of hydrogen production in a 10 MW_{th} two-stage gasification system using wood chips as feedstock. Mass and energy balances have been established in the Aspen Plus and MATLAB software. In contrast to most models in the literature, which were based on the equilibrium approach, the proposed system utilizes reliable kinetic models for the gasifier operation and the main downstream processes. An extensive validation of the gasifier kinetic model has been carried out and then a sensitivity analysis, which has revealed that the optimum steam-to-biomass ration (SBR) is 0.8 and 1.2 for the air-steam and the oxy-steam gasification systems, respectively. Further, the optimum steam-to-CO ratio (S/CO) for the water gas shift reactors (WGSRs) is 4, under which an overall 82.9% conversion of CO has been achieved. The results show that the 10 MW_{th} two-stage gasifier can attain a specific hydrogen yield of 81.47 gH_2/kg dry biomass. Based on the carbon footprint assessment, the process is net negative with an emission factor of −1.38 $kgCO_2$-eq/kg biomass. Further, heat integration has also been conducted and it was found that the energy conversion efficiency of the whole system is 49.6%. This study is important since it provides a reliable data source for biomass-based hydrogen production through gasification in a commercial two-stage gasifier that can dictate operational strategies of pilot and demo plants.

1. Introduction

The transition towards renewable and clean energy supplies is a necessity to combat climate change. Hydrogen can play a major role in this transition, and it is regarded as a prospective alternative to fossil fuels [1]. Also, this explains why, according to the International Energy Agency (IEA), hydrogen is an important piece of the energy puzzle to achieve the targeted net zero emissions by 2050 [2]. Besides its usage as fuel, hydrogen is also utilized in many chemical processes, such as fuel upgrading and the production of ammonia and methanol. Currently, most of the commercial hydrogen production (e.g., 94 Mt in 2021) is obtained from fossil fuel sources, that is 62% from natural gas, 18% from oil and refineries, and 19% from coal, while its production from low carbon sources is limited to 1%. Consequently, hydrogen production is CO_2 intensive with an emission factor of approximately 9.6 kg CO_2/kg H_2 [2]. Therefore, in order to boost the capacity of hydrogen production while maintaining the CO_2 emissions at low levels, renewable sources (e.g., biomass, wind and solar energy) should be utilized. Biomass is a renewable energy source with cumulative low, zero, or negative carbon emissions depending on the rate of growth vs the rate of consumption. Further, when the biomass energy conversion process (i.e., bioenergy) is integrated with carbon capture and storage (also known as BECCS), the contribution into the mitigation of climate change is even greater. In

* Corresponding author.
E-mail addresses: kelamawy1@sheffield.ac.uk, karim_rabea@yahoo.com (K. Rabea).

https://doi.org/10.1016/j.enconman.2023.117812
Received 1 August 2023; Received in revised form 4 October 2023; Accepted 26 October 2023
Available online 1 November 2023

Nomenclature

Abbreviations

BECCS	Bioenergy with Carbon Capture and Storage
CFBG	Circulating fluidized bed gasifier
CGE	Cold gas efficiency
CHP	Combined heat and power
d.a.f	Dry ash free
DFB	Dual fluidized bed
DG	Downdraft gasifier
DME	Dimethyl Ether
EF	Entrained flow
ER	Equivalence ratio
FC	Fixed carbon
HHV	Higher heating value
HTWGSR	High temperature water gas shift reactor
LHV	Lower heating value
LTWGSR	Low temperature water gas shift reactor
MC	Moisture content
ORC	Organic Rankine cycle
PG	Plasma gasifier
PSA	Pressure swing adsorption
RGibbs	Minimum Gibbs free energy reactor
RMSD	Root mean square deviation
RPlug	Plug flow reactor
SAF	Sustainable Aviation fuel
SBR	Steam to biomass ratio
VM	Volatile matter
WGSR	Water gas shift reactor
stoich	Stoichiometric

Symbols

A	Pre-exponential factor
[C]	Concentration
E	Activation energy
$H_{f,B}$	Enthalpy of formation for biomass
$h_{f,i}$	Enthalpy of formation of species i
h_{fg}	Latent heat of water
h_i	Sensible enthalpy of species i
K_P	Equilibrium constant
n	Reaction order
P_i	Partial pressure
S	steam
T_o	Reference temperature
wt.%	Weight percent
x	Mole fraction
X	Conversion
y	Mass fraction
ν_i	Moles of species i
$\dot{q}$	Rate of heat loss per unit mass of flow
$\dot{m}$	Mass flow rate
β	Heating rate

such systems, the biomass can be utilized for power generation or converted into various fuels and/or chemicals, such as syngas, Dimethyl Ether (DME), sustainable aviation fuels (SAF), and hydrogen [3,4]. With that in mind, BECCS represents a promising approach to achieving negative emissions. In addition, it is considered to be an economically viable option for low-carbon hydrogen production process compared to the other renewables-based alternatives [5]. One of the most promising energy conversion technologies of biomass is the thermochemical gasification, which exploits most of the energy content of solid biomass and converts it to a gaseous fuel (mainly, composed of CO, H_2, CO_2, CH_4 and C_xH_y) with a high conversion efficiency and a high hydrogen yield [6].

For the air-driven gasification systems, the hydrogen content in the produced gas can vary between 5 and 21 dry vol.% depending on various factors, such as the type of biomass being used, the gasifying agent, the design of the gasification reactor and other operating conditions [7,8]. In order to boost the hydrogen production in the produced gas, steam can be utilized as a gasifying agent. The steam addition can increase the H_2 content up to 54% at steam to biomass ratios (SBR) between 0.8 and 1.4 depending on other process considerations, especially the gasification temperature [9–12]. Further, it is common to intensify the hydrogen concentration in the produced gas by capturing the CO_2 during and/or after the gasification process. During the gasification process, it can be achieved through the in-situ sorption of CO_2 by a solid sorbent as investigated by [13,14]. However, this concept of hydrogen enrichment is still premature and has not been applied on large scales. The capture of CO_2 from the produced gas can be carried out after the gasification process, which opens the door for other various techniques, such as physical and chemical absorptions, and the membrane separation [15,16].

Similar to the current commercial plants, hydrogen production systems through BECCS can follow the same approach of hydrogen enrichment, i.e., they utilize water gas shift reactors (WGSRs) to convert the CO into H_2. Following that, typical gas separation technologies can be applied for high purity hydrogen recovery. For example, Spath et al. [17] investigated a biomass-based hydrogen production system based on the entrained flow (EF) gasifier from the test facility of Battelle Columbus Laboratory at a scale of 9 tonnes/day. The syngas from the gasifier was upgraded through a tar reformer, a desulfurization unit and two water gas shift reactors in series; then the hydrogen was separated by a pressure swing adsorption (PSA) unit. Whereas the off gas from the PSA is combusted along with natural gas to provide the heat required for the tar reformer, and the flue gas heat was integrated for steam generation. The gasifier was modeled in Aspen Plus by using the RYield reactor that incorporated experimental correlations from the relevant test runs. The tar reformer, the high temperature and the low temperature water gas shift reactors were simulated as equilibrium reactors. The overall system efficiency was 45.6%, where the gasifier cold gas efficiency was 71.8% (LHV based). The same approach for syngas upgrading was followed by Susmozas et al. [18], in which a dual fluidized bed (DFB) gasifier is employed to produce the syngas. A comparison between the types of gasifiers (i.e., oxygen-blown high pressure EF gasifier and the air-blown atmospheric pressure dual fluidized bed gasifier) for hydrogen production has been investigated by Salkuyeh et al. [6]. The thermal efficiency of the hydrogen production from the entrained flow gasifier was higher than that of the fluidized bed by 11%. This is due to the extra biomass needed for the combustor in the dual fluidized bed gasifier and this can be seen in the specific hydrogen production rate (64 and 77 gH_2 per kg of biomass for the DFB gasifier and the EF gasifier, respectively). These two types of gasifiers are the most commonly-studied systems for hydrogen and/or biofuel production as reported in [4,19–22].

Some other studies considered the bubbling fluidised bed gasification system for hydrogen production [23–25]. For instance, Ersoz et al. [23] investigated the production of high purity hydrogen from wood through a bubbling fluidized bed by using an Aspen Plus model to simulate the gasifier with the capacity of 100 kW_{th}. Similar to previous studies, the syngas was upgraded through a tar reformer, WGSRs, and PSA; all the system components were simulated under equilibrium-based operation. At this capacity (100 kW_{th}), the hydrogen production rate from this system was 76.1 gH_2/kg dry biomass. Similarly, Marcantonio et al. [25] simulated the hydrogen production from hazel nut shells through gasification in a bubbling fluidized bed reactor at a

capacity of 1 MW_{th}. The gasifier was simulated following a quasi-equilibrium approach in an RGibbs reactor and it was adjusted to match the experimental results through the restricted equilibrium control method. Two separation technologies have been considered and compared for H_2 recovery, i.e., PSA and palladium membrane. The hydrogen recovery ratio from the biomass was 38% and 49% by the PSA and the palladium membrane, respectively.

Further, Kalinci et al. [26] compared the hydrogen production from a downdraft gasifier (DG), a circulating fluidized bed gasifier (CFBG) and a plasma gasifier (PG), at different plant capacities. The specific hydrogen production rate was 54, 61.3, and 28.4 gH_2/kg biomass for the DG, the CFBG and the PG, respectively. The plasma gasification was the most power consuming at a rate of 19.38 MJ/kg of biomass, while for the CFBG and the DG, this was 1.336 MJ/kg and −0.709 MJ/kg of biomass, respectively. Also, Martins et al. [27] investigated the hydrogen production from biomass gasification through three different types of gasifiers, i.e., conventional gasifier, supercritical water gasifier, and plasma gasifier. They concluded that the supercritical water gasification-based system gives the highest specific yield of hydrogen at a rate of 0.844 Nm^3/kg of biomass, compared to 0.828 and 0.758 Nm^3/kg that were attained from the conventional gasifier and the plasma gasifier-based systems, respectively.

Since the gasifier is the driving force for the entire system, the quality of the syngas depends, to a great extent, on the adopted gasification technology [6]. Among the different designs, the multistage fixed bed gasification system has recently proved its competence to produce high quality syngas with minimum tar content, and its overall performance has outranked the conventional designs [28]. The commercial module of this design is developed by Xylowatt SA. under the name of the NOTAR® gasifier [29]. Considering this high-quality syngas, it represents a promising basis for the hydrogen production from biomass. This study is the first attempt to investigate the technical feasibility of this technology for hydrogen production through biomass gasification at a commercial scale (10 MW_{th} NOTAR gasifier) within the BECCS concept. Most modelling studies assume equilibrium conditions for the main system units, such as the gasifier and the WGSRs, but this approach lacks accuracy. Equilibrium models tend to underestimate the CO_2 and CH_4 contents, and overestimate the H_2 and CO contents [27,30]. In addition, the equilibrium models neglect the reactor geometry. To overcome these limitations, the current study utilizes a detailed, reliable kinetic model for the gasifier and the WGSRs, with the aim of achieving a comprehensive technical investigation and assessment of the system.

2. Materials and methods

2.1. Feedstock

Wood chips have been considered as the feedstock with initial moisture content of 30% that is reduced on-site via drying to 7.5%. Table 1 provides the proximate and ultimate analyses of the feedstock, which were carried out according to the XP CEN/TS 15,104 and the ASTM-D 5373 standards [31]. Based on the ultimate analysis, the feedstock can be formulated as $CH_{1.45}O_{0.66}$. The feedstock is introduced to the two-stage fixed bed gasifier to be processed for synthetic gas (syngas) production.

Table 1
Proximate and ultimate analyses of wood chips [31].

Proximate analysis (wt.%)				Ultimate analysis (wt.%, dry basis)				
MC	VM dry basis	FC	Ash	C	H	N	S	O
7.5	81.8	16.9	1.3	49.1	5.94	0.2	0.05	43.41

2.2. Description of the two-stage fixed bed gasifier

The principle of the continuous two-stage fixed bed gasification reactor relies on decoupling the gasification zones (pyrolysis and char gasification). This approach of staged gasification allows for better control of the pyrolysis products as well as enabling the independent optimization of the two stages [32]. Herein, we have utilized the NOTAR technology, which integrates the advantage of the staged gasification with the advantage of the multi air supply but in a compact configuration as shown in Fig. 1 [31]. This integration contributes to achieving minimum tar content in the product gas and consequently minimal gas processing [28,33]. Compared to the other types of gasifiers, the two-stage gasifier is technically ranked as the second top after the plasma gasifier, and it outranks the other types of gasifiers, i.e., fixed bed, fluidized bed and the entrained flow gasifiers [28]. Therefore, it can be considered as a promising technology for hydrogen production. In addition, it is expected to be an economically viable option when compared to plasma gasification.

2.3. The gasification kinetic model

The two-stage gasification reactor is modelled through a detailed kinetic model that accurately simulates the gasifier performance. In principle, during the gasification process in a fixed bed gasifier, the biomass particles are processed as they move through the different temperature zones. It starts with the drying of the particles, as the moisture content is the first to be released, then the particles' components start to decompose at higher temperatures by releasing gases and

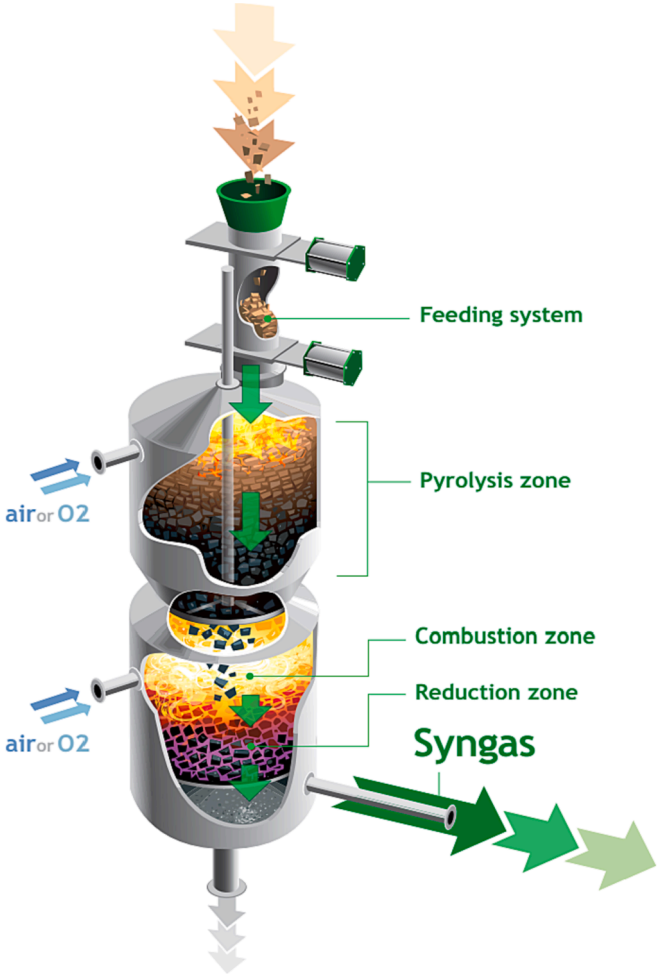

Fig. 1. The Notar two-stage gasifier [34].

tar. This stage is known as the pyrolysis stage. The released water vapor, tar and gases interact with each other and react with the solid char as well as with the gasifying agent that is introduced to the reactor.

The developed model considers the consecutive release of the pyrolysis non-condensable gases depending on the temperature. CO_2 is the first to leave the biomass particle at the early stage of pyrolysis. Then, the CO and the CH_4 are to be released at a relatively higher temperature followed by the H_2 as the final non-condensable gas component to leave the biomass particle. This consecutive release of the non-condensable gases is governed by the temperature in the reactor, which in turn controls their contribution in the homogeneous reactions. The evolution of the pyrolysis gases and the temperature profile are simulated in MATLAB, which is integrated with the Aspen Plus software to model the gasifier operation. This approach of modelling has proved its accuracy to simulate the gasification process in the downdraft gasifier and the updraft gasifier [35,36]. The flow chart of the integrated modelling approach for the gasifier is presented in Fig. 2.

The distribution of the products from the biomass decomposition is obtained from the pyrolysis of wood at 800 °C as studied by Tanoh et al. [37] and can be represented as follows:

$$\text{woodchip}\ (CH_{1.45}O_{0.66}) \rightarrow 0.127\text{char} + 0.107CO_2 + 0.211CO + 0.237H_2O + 0.16H_2 + 0.106CH_4 + 0.029C_2H_4 + 0.0516\text{Tar} \quad (1)$$

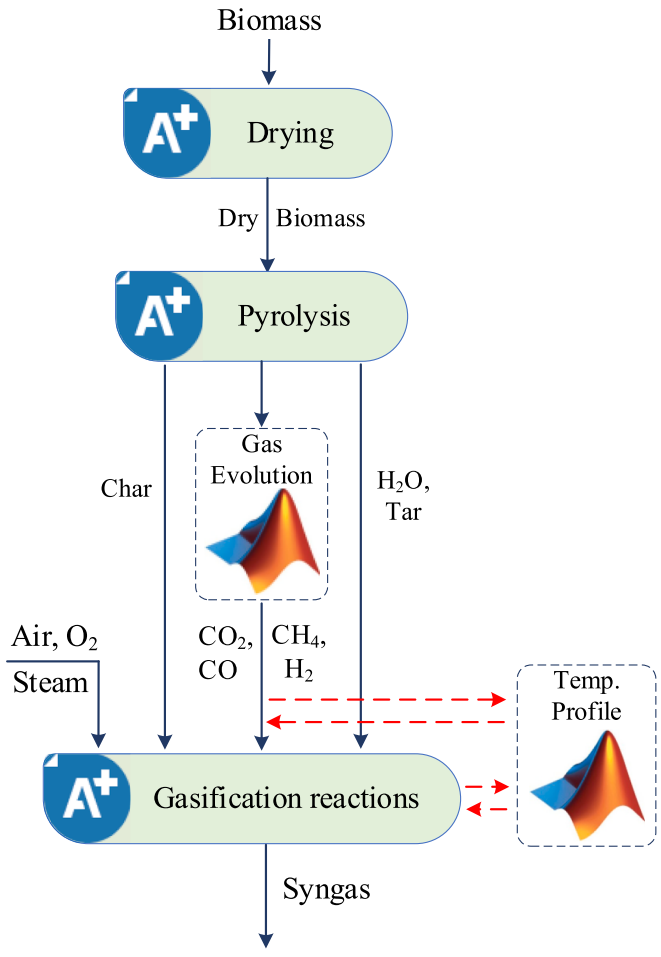

Fig. 2. The flow chart of the Aspen Plus/MATLAB integrated modelling approach for the gasifier.

Table 2
The Single Reaction Model for the non-isothermal pyrolysis [35,38].

The time-based and temperature-based rate equations

$$\frac{dx}{dt} = k(1-x)^n, x = \frac{v_i}{v_i^*} \quad (2)$$

$$\frac{dx}{dT} = \frac{A}{\beta}\exp\left(\frac{-E}{RT}\right)(1-x)^n \quad (3)$$

	Kinetic parameters		
Gas Component	E (J/mole)	A (min^{-1})	Reaction order (n)
CO_2	43,300	915.63	2
CO	37,810	33.75	2
CH_4	50,740	335.62	2
H_2	60,570	220.49	2

To simulate the consecutive release of the non-condensable gases, the Single Reaction Model is utilized. The rate equation of this model, along with the kinetic parameters for each gas component, are tabulated in Table 2. The equation of the temperature-based rate of pyrolysis gas evolution is solved in MATLAB by utilizing the embedded solver (ode45) and the results are exported to Aspen Plus to take part in the gasification reactions. The introduction of the gases into the gasification reactions is governed by the temperature, which is also simulated in MATLAB and applied into the Aspen Plus model. The interaction between MATLAB and Aspen Plus is outlined in Fig. 2. More details about the pyrolysis gas evolution and the single reaction model and how it is applied and solved in MATALAB can be found in [35].

The pyrolysis products are introduced to the Aspen Plus model, where the gasification reactions, i.e., the combustion and reduction reactions, are modelled by seven RPlug reactors as discussed in section 2.4.1. In this model, the tar is simulated as a combination of benzene, toluene, and naphthalene, which represent the major compounds of tar from wood at 800 °C as reported in [37,39]. Their relative fractions are assumed to be 64.6%, 12.6%, and 22.8%, respectively [37]. Table 3 presents the chemical reactions of the gasification process along with the respective kinetic parameters.

2.4. The Aspen plus model for H_2 production

2.4.1. Pretreatment and gasification

The Aspen Plus simulation starts by defining all the components involved in the simulation by selecting the conventional components from the library, whereas the woodchips, char and tar are defined as non-conventional components. These components are recognized through their elemental analysis (C, H, N, O, S) [52]. The properties of these components, such as the enthalpy and the density, are evaluated by the built-in models, known as the HCOALGEN and DCOALIGT models, respectively. For the conventional materials, the properties are evaluated by the Peng Robinson method with Boston Mathis alpha function (PR-BM), which is advised to be used for the gas and petrochemical processes. The Peng-Robinson equation of state is well-known to be successfully applied for thermodynamic and volumetric calculations of pure compounds and mixtures. Boston Mathias alpha is an improved version of the original alpha in the Peng Robinson equation, which enhances the temperature-dependent variation of properties [53]. For water and refrigerant streams, the selected property methods are STEAM-TA and REFPROP, respectively. The process flow diagram of the gasifier model is shown in Fig. 3. The woodchips are first dried from

Table 3
Chemical reactions and kinetic parameters.

Reaction		Kinetic parameters		
		A (s^{-1})	E (J/mol)	Ref.
R1	$C + 0.5O_2 \rightarrow CO$	$2.3\,T \times [O_2]^{0.4}$	92,300	[40]
R2	$C + O_2 \rightarrow CO_2$	2512	53375.9	[41]
R3	$C + CO_2 \rightarrow 2CO$	$4.4\,T \times [CO_2]^{0.6}$	162,000	[40]
R4	$C + H_2O \rightarrow CO + H_2$	15,170	121,620	[42]
R5	$C + 2H_2 \rightarrow CH_4$	4.189×10^{-3}	19200	[43]
R6	$CO + 0.5O_2 \rightarrow CO_2$	$1.3 \times 10^8 [H_2O]^{0.5} [CO]^1 [O_2]^{0.25}$	125,591	[44]
R7	$CO + H_2O \leftrightarrow CO_2 + H_2$	2780	12,560	[45]
	Reverse	95,862	46637.5	[45]
R8	$CH_4 + H_2O \leftrightarrow CO + 3H_2$	6.09×10^{14}	257,000	[46]
	Reverse	312	30,000	
R9	$H_2 + 0.5O_2 \rightarrow H_2O$	2.2×10^9	109,000	[47]
R10	$CH_4 + 1.5O_2 \rightarrow CO + 2H_2O$	$5.0119 \times 10^{11} [CH_4]^{0.7} [O_2]^{0.8}$	202,504	[41]
R11	$C_2H_4 + O_2 \rightarrow 2CO + 2H_2$	$2.73 \times 10^{11} [C_2H_4]^{0.9} [O_2]^{1.18}$	200841.3	[48]
R12	$C_2H_4 + 2H_2O \rightarrow 2CO + 4H_2$	3100.5	124,710	[49]
R13	$C_6H_6 + 4.5O_2 \rightarrow 6CO + 3H_2O$	3.8×10^7	5545	[50]
R14	$C_6H_6 + 2H_2O \rightarrow 1.5C + 2.2CH_4 + 2CO$	$3.39 \times 10^{16} [C_6H_6]^{1.3} [H_2O]^{0.2} [H_2]^{-0.4}$	443,000	[50]
R15	$C_7H_8 + 3.5O_2 \rightarrow 7CO + 4H_2$	$1.3 \times 10^{11} [O_2]^{0.5} [H_2O]^{0.5}$	125,600	[50]
R16	$C_7H_8 + 10{\cdot}.5H_2O \rightarrow 3.5CO_2 + 14.5H_2 + 3.5CO$	232,300	356,000	[50]
R17	$C_{10}H_8 \rightarrow 9C + 0.1667C_6H_6 + 3.5H_2$	$3.39 \times 10^{14} [C_{10}H_8]^{1.6} [H_2]^{-0.5}$	350,000	[51]
R18	$C_{10}H_8 + 7O_2 \rightarrow 10CO + 4H_2O$	$9.2 \times 10^6 T [C_{10}H_8]^{0.5} [O_2]$	80,000	[50]
R19	$C_{10}H_8 + 4H_2O \rightarrow C_6H_6 + 4CO + 5H_2$	268,000	95,700	[51]

30% to 7.5% moisture content by utilizing the heat generated within the system. This pre-gasification drying process is simulated in an RStoic reactor by following the reaction as follows [54]:

$$Biomass_{wet} \rightarrow 0.0555H_2O \quad (4)$$

This reactor enables the calculation of the energy demand needed for a specified conversion of biomass into water vapor. Here, in order to achieve the 7.5% value, the conversion of biomass is 22.5%. This equation implies that the biomass is converted to 1 kg of water, and this is based on the biomass molecular weight being recognized as 1 kg by Aspen Plus, since it is a non-conventional component. Following this, the wood chips are converted to conventional components, i.e., H_2O, C, O_2, H_2, S, N_2 and Cl_2 through an RYield block "DECOMPOS", while maintaining the mass conservation of the ultimate analysis of the wood chips [55]. The decomposed components are directed to another RYield block, which is governed by a FORTRAN calculator to simulate the pyrolysis process according to equation (1) at 800 °C. It should be noted that the composition of the tar is identified according to the previously mentioned fractions of benzene, toluene, and naphthalene. In order to maintain the mass conservation of the woodchips, the elemental composition of the char is identified by determining the residual mass fractions of C, H, and O and they are calculated in another FORTRAN block "PYROL1". All the FORTRAN codes can be found in the supplementary material.

The gasification reactions are simulated in seven RPlug reactors connected in series, which are configured to match the reactor dimensions. The pyrolysis gas components are introduced to the RPlug reactors through the separator block "GAS-EVOL" according to the temperature-based gas evolution model (see Table 2). The temperatures of the gasifier reactor (i.e., the RPlug reactors) are modelled in MATLAB by applying the energy conservation principle over the different gasification zones. The energy balance equations are presented in Table 4, where T_{pyr}, T_{comb}, and T_{red} are the temperatures of the pyrolysis, the combustion, and the reduction zones, respectively. Also, the term for the heat loss rate in the energy equations ($\dot{q}$) is a function of the equivalence ratio (ER) and the lower heating value (LHV) as reported in the literature [56,57]. It is estimated as 0.08, 0.1, and 0.32 of the product (ER × LHV) for the pyrolysis, the combustion, and the reduction zones, respectively. These numbers represent lower heat loss assumptions than those

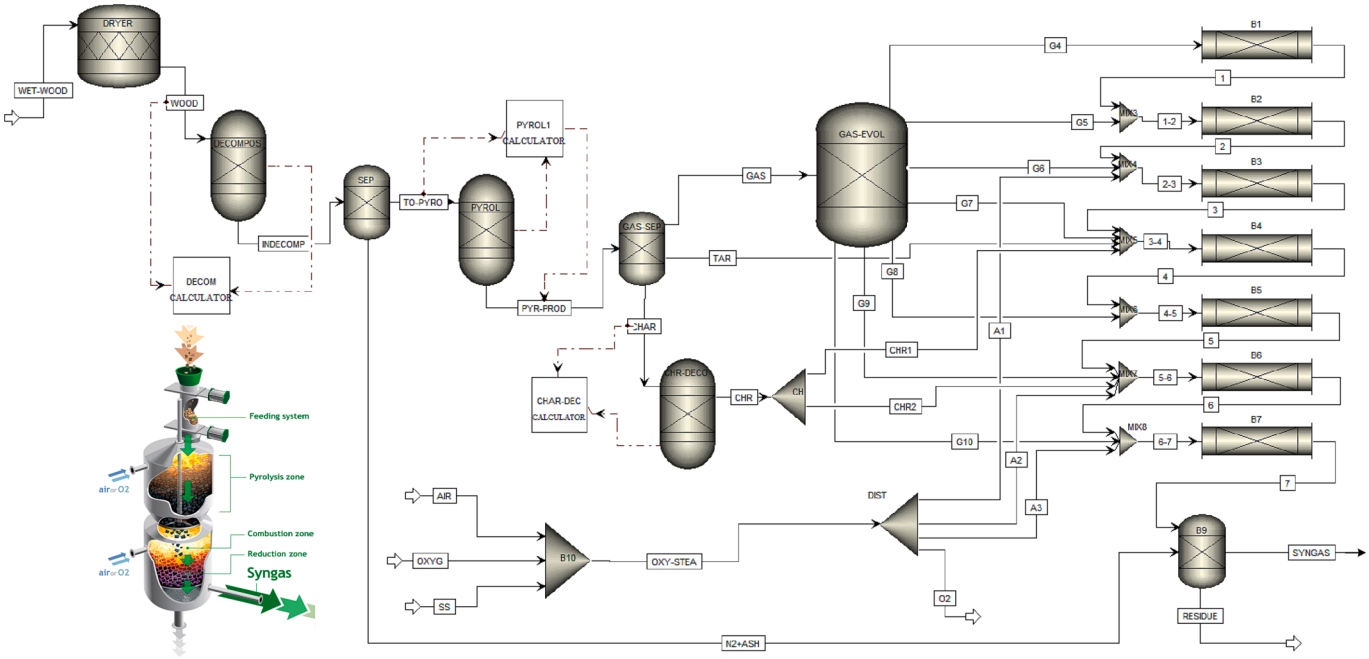

Fig. 3. Process flow diagram of the two-stage gasifier.

Table 4
Equations for the energy balance model [35].

Energy balance (Pyrolysis zone)	$\dot{H}_{f,B}(T_o) + \dot{H}_{f,agent} = \sum_{i,out}\dot{m}_i\left[h_{f,i}(T_o) + h_i(T_{pyr}) - h_i(T_o) + \dot{q}_{pyr}\right]$	(5)
Energy balance (Combustion zone)	$\dot{H}_{f,B} + \dot{H}_{f,agent} = \sum_{i,out}\dot{m}_i\left[h_{f,i}(T_0) + h_i(T_{comb}) - h_i(T_o) + \dot{q}_{comb}\right]$	(6)
Energy balance (Reduction zone)	$\dot{H}_{f,B} + \dot{H}_{f,agent} = \sum_{i,out}\dot{m}_i\left[h_{f,i}(T_0) + h_i(T_{red}) - h_i(T_o) + \dot{q}_{red}\right]$	(7)
Enthalpy of formation for biomass (wet and dry)	$\dot{H}_{f,B} = \dot{m}_B\left[(1-\mathrm{MC}) \times h_{f,\mathrm{DB}}(T_o) + \mathrm{MC} \times h_{f,\mathrm{MC}}(T_o)\right]$	(8)
	$h_{f,DB}(T_o) = \mathrm{HHV} + \left[Y_C \times h_{f,CO_2}(T_o) + 0.5 \times Y_H \times h_{f,H_2O}(T_o)\right] - \left[(A/F)_{stoic} \times h_{f,O_2}(T_o)\right]$	(9)
Biomass HHV	$\mathrm{HHV}_{biomass} = 0.3419\mathrm{C} + 1.1783\mathrm{H} + 0.1005\mathrm{S} - 0.1034\,\mathrm{O} - 0.015\,\mathrm{N} - 0.0211\,\mathrm{Ash}$	(10)
Biomass LHV	$\mathrm{LHV}_{biomass} = \mathrm{HHV} - h_{fg} \times (9Y_H + Y_{\mathrm{MC}})$	(11)
Equivalence ratio	$\mathrm{ER} = \dfrac{\left[\dot{m}_{air}/\dot{m}_B\right]_{actual}}{\left[\dot{m}_{air}/\dot{m}_B\right]_{stoich}}$	(12)
Stoichiometric Air-fuel ratio	$\left[\dfrac{\dot{m}_{air}}{\dot{m}_{biomass}}\right]_{stoich} = \dfrac{1.293}{0.21}\left(1.866\dfrac{\mathrm{C_{daf}}}{100} + 5.55\dfrac{\mathrm{H_{daf}}}{100} + 0.7\dfrac{\mathrm{S_{daf}}}{100} - 0.7\dfrac{\mathrm{O_{daf}}}{100}\right)$	(13)

reported in the study of Diyoke et al. [56]. Further details about modeling the temperatures of the zones in MATLAB and how the data are exchanged with Aspen Plus can be found in [35].

When the RPlug reactors simulate kinetic-based chemical reactions, they take into account the dimensions of the reactor and the temperature profile along the reactor length. The dimensions of the two-stage gasifier are adopted from a scaled-down gasifier unit, i.e., NOTAR gasifier at a syngas-based capacity of 200 kW_{th} [31]. The internal diameter of the reactor is 0.6 m and the total height of the gasifier plant is approximately 3 m. The dimensions of the gasifier are applied into the RPlug reactors (B1 to B7 in Fig. 3) based on the actual passage that the biomass goes through during the gasification process. This is such that the top five RPlug reactors are designated to simulate the reactions in the pyrolysis zone with a height of 0.18 m per block. Then, the combustion and reduction zones are simulated by the 6th and the 7th blocks with heights of 0.35 m and 0.6 m, respectively. The gasifying agents (air, oxygen, and/or steam) are supplied to the reactors through a stream distributer "Dist" to provide the gasifying agents to the stages of the gasifier. A1 is the 1st stream to introduce the agents to the pyrolysis zone with a variable split fraction between 0.23 and 0.38 as per the operating condition of the gasifier [31]. The 2nd main split stream of the agents is A2, which takes a fraction of 0.4 from the main flow to the combustion reactor (B6), while the remaining flow goes to the reduction reactor B7 through A3. The last stream is considered to represent the permeating agents through the biomass bed [35]. The residual ash and carbon are separated by block B9 as shown in Fig. 3, while the produced syngas is

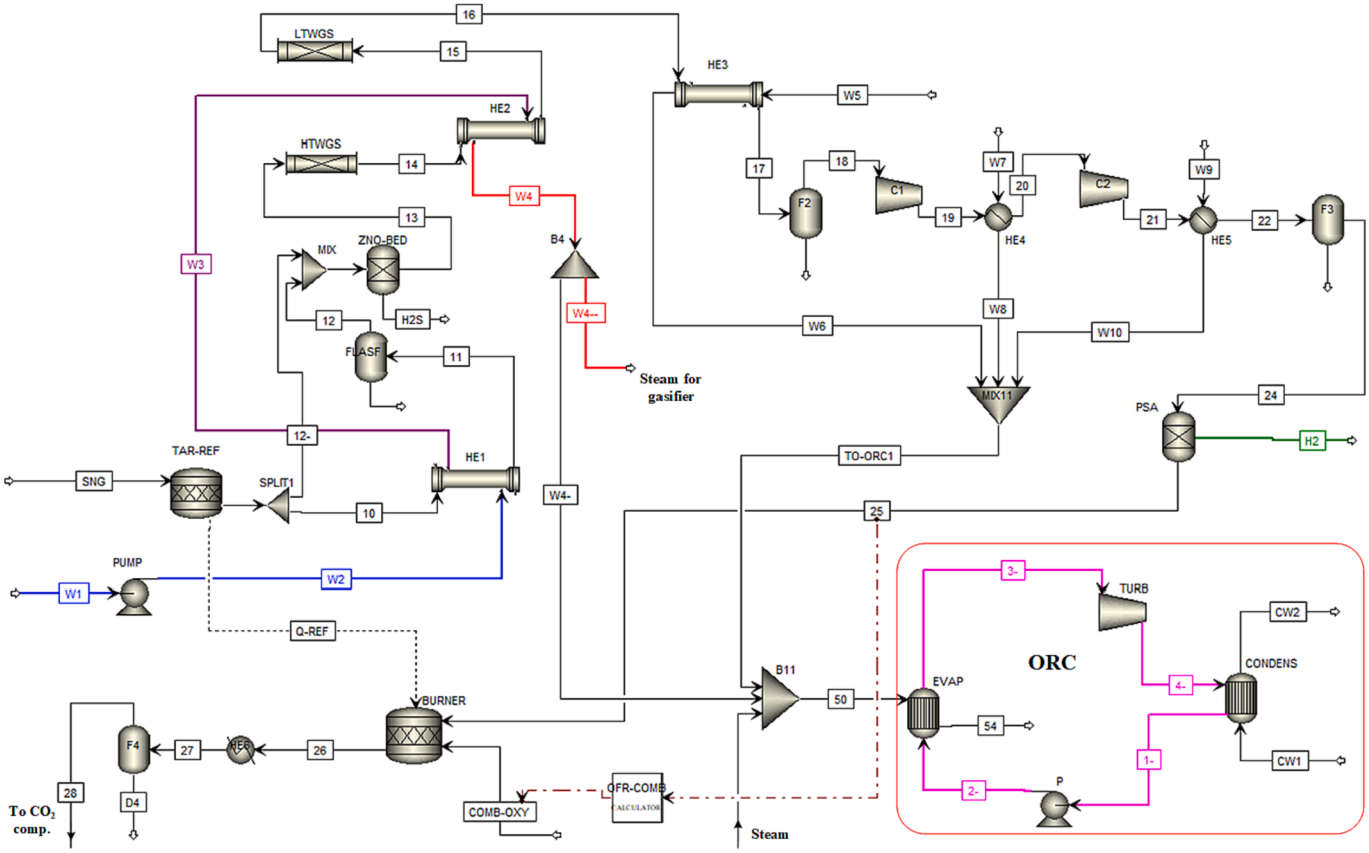

Fig. 4. Process flow diagram of syngas upgrading to hydrogen production and the heat integration network.

Table 5
Catalytic reaction rate of the HTWGS and LTWGS reactions.

Reactor	Catalyst	Inlet Temp.	Reaction rate	Ref.
HTWGS	Fe-Cr	450 °C	$r = 4.56exp(\frac{-88}{RT}) \times \frac{(P_{CO})^{0.9}(P_{H_2O})^{0.31}}{(P_{CO_2})^{0.156}(P_{H_2})^{0.05}} \times (1-\beta^*)$	[59]
LTWGS	CuO/ ZnO/ Al_2O_3	230 °C	$r = 4.785exp(\frac{-34.983}{RT}) \times \frac{(P_{CO})^{0.854}(P_{H_2O})^{1.99}}{(P_{CO_2})^{1.926}(P_{H_2})^{0.573}} \times (1-\beta)$	[62]
$\beta^* = \frac{[CO_2][H_2]}{[CO][H_2O]K_P}$, $K_P = exp(\frac{4577.8}{T} - 4.33)$				[63]

directed to the downstream chemical processing units as depicted in Fig. 4. Prior to the gas upgrading, the gas flow and accordingly the size of the chemical processing plant are scaled to 10 MW_{th} syngas power by considering five modular units of a 2 MW NOTAR gasifier [58]. This is equivalent to a total biomass feeding rate of 2,975 kg/h on a wet basis.

2.4.2. Syngas upgrading model

The downstream process that follows the syngas production includes the gas reforming, H_2 enrichment through WGS reactors, and the recovery of H_2. Also, the model considers the heat and energy integration between the system components. The produced gas is firstly directed to a tar reformer to convert most of the remaining tars into CO and H_2 using steam according to the following equation:

$$C_nH_m + nH_2O \rightarrow nCO_2 + \left(n + \frac{m}{2}\right)H_2 \quad (14)$$

This reformer is simulated as a RStoic reactor at 900 °C with fractional conversion values of 89.4%, 93.6% and 95% for benzene, toluene and naphthalene, respectively [17,39]. The heat required by this reformer is supplied by the burner "Burner" which uses the PSA off gas as the fuel source as shown in Fig. 4. The hot reformed syngas is then cooled down to 450 °C, which is the targeted temperature for the catalytic high temperature water gas shift reactor (HTWGSR) [59]. This temperature is achieved by splitting the hot syngas into two streams, where only one of them is cooled down by water in the 1st heat exchanger (HE1). The split fraction is adjusted to meet the required temperature of the HTWGSR after mixing the two streams again. Furthermore, the split fraction and the design specification of the heat exchanger can be adjusted to control the condensation of steam in the syngas stream, which is reflected onto the steam to the CO ratio in the mixed gas for the HTWGSR. For this model, the split fraction is 0.63 of the syngas and this is directed to the cooling heat exchanger, for which the design specification is "Hot stream outlet temperature = 75 °C".

It is worth mentioning that a ZnO bed is utilized to remove the H_2S from the syngas before the HTWGS reactor. The partially shifted gas is then cooled further down to 230 °C through the 2nd heat exchanger (HE2) before the low temperature water gas shift reactor (LTWGS). The cold stream in the 1st and the 2nd heat exchangers is heated to produce the steam required for the steam gasification process. Meanwhile, the hydrogen content in the relatively cooled syngas is enriched more through the LTWGS reactor. Two RPlug reactors with catalysts are employed to simulate the WGS reactors under adiabatic conditions [60], where the kinetic rate expressions of the catalytic reactions are presented in Table 5. The bulk density of the catalyst bed and the bed voidage are assumed to be 1400 kg/m^3 and 0.5, respectively and this lies in the range reported in the literature [61]. The WGS is a reversible reaction as shown in equation (15) and it is simulated in Aspen Plus with the reaction class of power law:

$$CO + H_2O \leftrightarrow CO_2 + H_2 \quad (15)$$

The shifted syngas is then cooled down to below its dew point to release out the residual water and to decrease the gas specific volume ahead of the compression process for the PSA unit. The gas compression is carried out in two stages at a pressure ratio of 4 for both stages and with isentropic and mechanical efficiencies of 85% and 95%, respectively. The PSA unit can produce hydrogen with a quality of 99.9% and a recovery rate of 80% [17]. It is simulated as a separator block in the Aspen Plus model, where the off gas is directed to the burner for combustion to supply the heat required for the tar reformer as depicted in Fig. 4. This burner is simulated as an RStoic reactor, and the stoichiometric mass flow rate of oxygen needed for this combustion is estimated in a calculator block "OFR-COMB" using the following equation:

$$Oxy_{comb}(kg/h) = 0.5712 \times CO + 7.9367 \times H_2 + 3.9892 \times CH_4 + 3.4218 \times C_2H_4 + 3.0723 \times C_6H_6 \quad (16)$$

The remaining sensible heat available in the flue gas, after supplying the necessary heat to the tar reformer, is utilized for the biomass drying prior to the gasification process.

2.4.3. CO_2 compression

The products from the oxy-combustor "BURNER" are mainly CO_2 and water vapor. This stream is cooled down and the moisture is rejected through the flash block (F4) before compression. Then, a series of compression stages with intercooling and flash separators are employed to compress CO_2 at supercritical conditions that are necessary for transportation. Fig. 5 depicts the three stages of compression (C3-C5), in which the final pressure of each stage is 7, 24, and 83 bar [64]. Following each compression stage, the compressed gas is cooled down with cooling water (W11, W13, or W15) and the condensate is knocked out in the flash blocks (F5, F6, or F7). Finally, the CO_2 stream is at 30 °C and 83 bar, which is above the critical pressure of 73.8 bar, and therefore the stream is in the liquid phase. Consequently, a pump is employed to pressurize the liquid CO_2 until it reaches the pressure of 153 bar that is required for the transportation in pipelines [64]. The isentropic and mechanical efficiencies of the compressors are 85% and 95%, respectively.

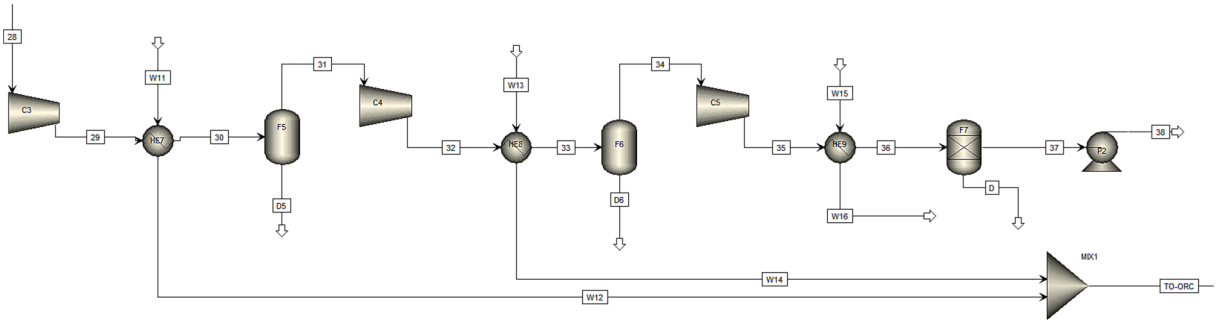

Fig. 5. Flow diagram of the multistage compression of CO_2.

Table 6
Specifications of the implemented ORC [68,69].

Working fluid	R245fa
Evaporator pressure	12.65 bar
Condenser pressure	2.42 bar
Pump efficiency	0.8
Turbine efficiency	0.75
Evaporator temperature	100 °C
Condenser temperature	39 °C
Superheating at evaporator exit	0 °C
Subcooling at condensation exit	0 °C

The hot water streams (W6, W8, W10, ……W14) are collected, and since the accumulated heat content is not high enough to run a steam turbine, an Organic Rankine Cycle (ORC) is utilized as can be seen in Fig. 4. It is worth mentioning that the water stream (W16) is not directed to the ORC, and this is due to its low temperature (i.e., 68 °C), that was achieved in the heat exchanger (HE9) without temperature cross over.

2.4.4. ORC modelling

In order to complete the heat integration of the entire process, the accumulated heat that is collected by the cooling water from the different units throughout the process, is utilized to run an ORC. The refrigerant R245fa is selected as the working fluid in the cycle owing to its preferred thermodynamic properties [65]. In addition, it is more safe and has a limited environmental impact due to its non-toxicity, low flammability and low effect on ozone depletion [66,67]. Two heat exchangers (i.e., the evaporator and the condenser), a pump and a turbine are employed to simulate the ORC. The heat sink of the cycle is cooling water at 20 °C, which exits the condenser at 37.5 °C. The specifications of the ORC are presented in Table 6. The corresponding flow rates of the refrigerant and the cooling water are estimated based on the available heat duty that is obtained from the process. Based on the hot water flow rate of 6.366 kg/s at the temperature of 119 °C, the refrigerant flow rate is estimated as 3.2 kg/s and the cooling water flow rate in the condenser as 7.7 kg/s.

3. Results and discussion

3.1. Model validation

The gasifier model is thoroughly validated by comparing the model results with the experimental data at different operating conditions and at different scales. In order to quantitatively evaluate the accumulated deviation between the model and the experimental results, the root mean square deviation (RMSD) is employed and this can be calculated as follows:

$$\mathrm{RMSD\,(vol.\%)} = \sqrt{\frac{\sum_{i=1}^{n}(X_{i,exp} - X_{i,mod})^2}{n}} \quad (17)$$

where, X_i represents the volume extent of each component (i) in the producer gas from the experiment and from the model. Table 7 shows a comparison of the gas composition between the model and the experimental results at different power conditions (162–217 kW_{th}) [31]. It can be seen that the model predictions are in very good agreement with the experimental data, where the RMSD varies between 0.53 and 0.76 vol%. These RMSD values are much better than the values reported for other models in the literature [70]. For instance, the equilibrium-based gasification model of Tauqir et al. [71] has reported an RMSD value of 2.53 vol%. Also, the kinetic-based model from Beheshti et al. [48] estimated an RMSD of 1.86 vol%.

Also, Table 7 shows how the increase in operational power is directly affecting the producer gas composition. When the air flow rate changes from 47.0 to 64.4 kg/h, the CO_2, H_2, and the CH_4 contents slightly decrease whereas the CO content slightly increases. These changes in the composition are a result of the change in residence time (reduced) and temperature (increased). The residence time reduces because of the increased flow velocity, and the temperature increases because of the increased heat release at higher air flow rates. Both effects tend to favor the partial oxidation of carbon to CO (R1) over the full oxidation to CO_2 (R2). Also, the hydrogasification reaction (R3) is known as the slowest, which leads to the reduction of CH_4 [72]. Another effect of the increased temperature is the promotion of the reverse water gas shift reaction (R7), which in turn reduces the hydrogen content in the syngas produced. This performance matches well the results reported in [73].

3.2. Validation of the scalability of the gasifier

In order to extend the validity of the model to represent the higher capacity of the gasifier, further validations have been carried out. Fig. 6 shows the model prediction in comparison to the experimental results at different capacities of the gasifier (i.e., 200 and 600 kW_{th}). In general, the model prediction of the gas composition shows a good agreement with the two capacities. Despite the underestimation of CO and CH_4 for

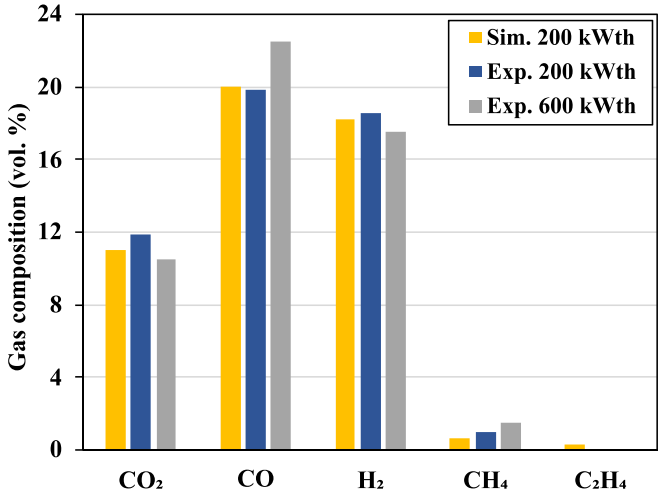

Fig. 6. Comparison of the gas composition between the model the experimental results of air gasification at 200 kW_{th} and 600 kW_{th} capacities [34].

Table 7
Validation of the two-stage gasification model with the experimental data from [31].

	Power = 162 kW_{th} Air = 72 Nm^3/h Biomass = 47.0 kg/h		Power = 169.25 kW_{th} Air = 78 Nm^3/h Biomass = 51.0 kg/h		Power = 217 kW_{th} Air = 96 Nm^3/h Biomass = 64.4 kg/h	
Parameter	Simulation	Experimental	Simulation	Experimental	Simulation	Experimental
CO_2 (vol.%)	11.25	12.49	11.15	11.85	10.98	11.89
CO (vol.%)	19.70	19.77	19.84	19.06	20.00	19.84
H_2 (vol.%)	18.41	19.30	18.25	19.13	18.24	18.54
CH_4 (vol.%)	0.46	1.16	0.44	0.83	0.33	1.00
RMSD (vol.%)	0.76		0.63		0.53	

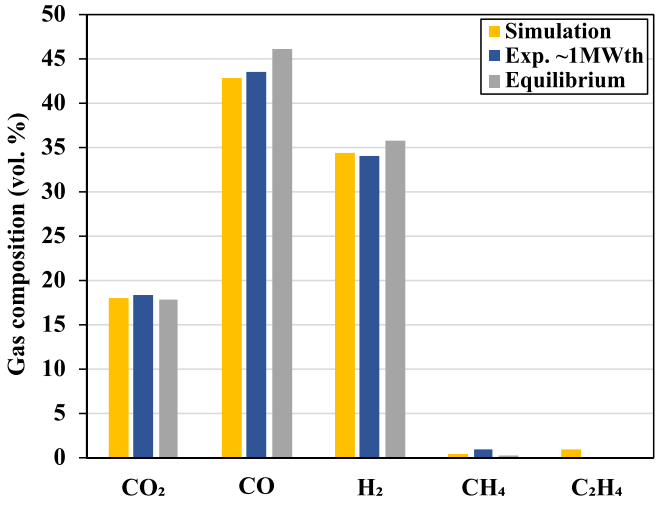

Fig. 7. Comparison of the kinetic model and the equilibrium model predictions against the experimental results of the 1 MW_{th} oxy-gasification in the NOTAR gasifier [34].

the high capacity, the overall RMSD is still good at 1.21 vol%. Also, it is worth noting that the model results show that a fraction of C_2H_4 is included in the produced gas and if it is added to the CH_4, the deviation of the simulation value from the experimental one would be reduced.

Further, it is essential to validate the model against experimental data from the gasifier under the condition and at the capacity that will be utilized for the hydrogen production process. Fig. 7 depicts the comparison between the model results and the 1 MW_{th} oxygen-based NOTAR gasification system which is designed to produce a nitrogen-free syngas by using oxygen instead of air as the gasifying agent. This oxygen is obtained from a cryogenic air separation unit, and it is introduced to the gasification process as 95% oxygen and 5% nitrogen. The oxygen flow rate and the corresponding biomass feeding rate for that scale are estimated as 100.6 Nm^3/h and 297.5 kg/h, respectively. It can be seen that the CO concentration has doubled, whereas the H_2 and CO_2 have increased by about 88% and 65%, respectively. Overall, the predicted dry volume fractions of the different gas components by the kinetic model are very close to the experimental values, in which the RMSD is estimated as 0.57 vol%. In addition, since most of the studies in literature employ the equilibrium model, another model is built in Aspen Plus based on the RGibbs reactor for comparison. The details of the equilibrium model can be found in the supplementary material. The results from the equilibrium-based gasification model at 900°C as well as from the kinetic model against the experimental results are presented in Fig. 7. It can be observed that the equilibrium model (RMSD = 1.47 vol%) is not as accurate as the kinetic model. It is important to notice that the equilibrium model overestimates both H_2 and CO concentrations and this will lead to a higher overestimation of the final H_2 yield (after the WGS) since the CO will be shifted to H_2.

3.3. *Effect of SBR on the gasification process.*

Steam-assisted gasification is very helpful for the hydrogen production from biomass, since the increase of steam provides abundance of H_2O for the water gas shift, and the methane reforming reactions [74]. The increase of the steam to biomass ratio (SBR) has a positive effect on the hydrogen content in the syngas, but the excess water vapor in the syngas causes temperature drop in the reactor as observed in [75,76] too. Hence, a parametric study on the effect of SBR on the air/steam and the oxygen/steam gasification has been carried out to achieve the optimum operating conditions of steam gasification. The SBR is a ratio of the total water content involved in the gasification process, (i.e., the steam released from the biomass and the pure steam introduced to the gasification process) to the dry biomass feeding rate, and it is calculated as follows [76]:

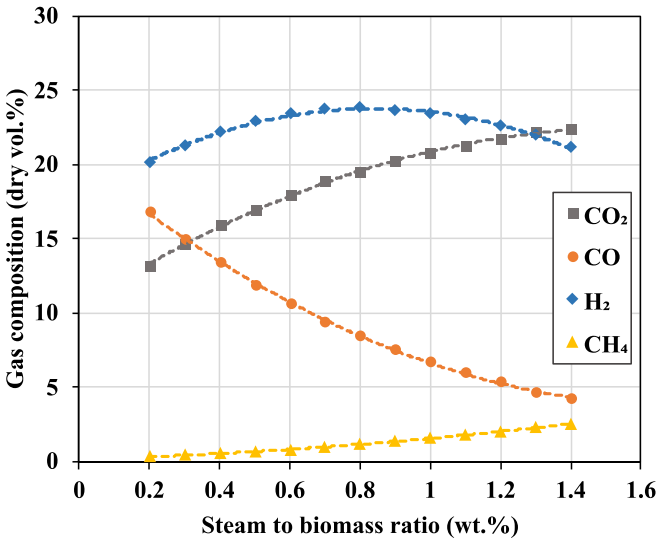

Fig. 8. Effect of SBR on the produced gas composition from the air-based gasification process.

$$SBR = \frac{\dot{m}_{steam} + \dot{m}_{moisture}}{\dot{m}_{drybiomass}} \quad (18)$$

3.3.1. *Steam-assisted air gasification*

For the case of air–steam, Fig. 8 shows how the dry-based gas composition changes with the increase in the amount of steam introduced to the gasifier at different SBRs. It can be seen that the H_2 and the CO_2 fractions increase from about 20.0% and 13.0% to 23.8% and 19.5%, respectively when the SBR increases from 0.2 to 0.8, while on the other hand, the CO declines from about 16.8% to 8.5%. As previously mentioned, this trend in the changes is expected as the introduction of more steam boosts the water gas shift reaction. However, beyond the SBR of 0.8, the hydrogen content starts to drop and a noticeable increase in the CH_4 is detected and this is attributed to the drop in the gasification temperature due to the excess of steam [75].

In addition, it is important to relate the change in the gas composition to the process evaluating parameters i.e., the lower heating value (LHV) of the producer gas and the cold gas efficiency (CGE), which can be calculated as follows [77,78]:

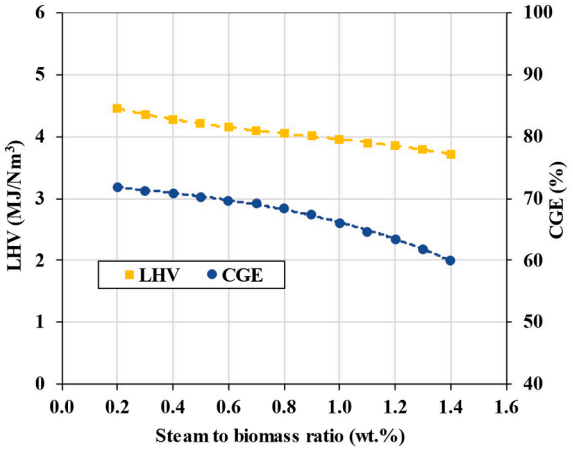

Fig. 9. Effect of SBR on the produced gas heating value and the efficiency of the air-based gasification.

$$\mathrm{LHV_{gas}}\left(\mathrm{MJ/Nm^3}\right) = [(10.79 \times \mathrm{H_2}) + (12.636 \times \mathrm{CO}) + (35.82 \times \mathrm{CH_4})] \quad (19)$$

$$\mathrm{CGE}\,\% = \frac{\dot{V_{gas}} \times [\mathrm{LHV}]_{\mathrm{gas}}}{\dot{m_B} \times [\mathrm{LHV}]_{\mathrm{biomass}}} \times 100\% \quad (20)$$

where, H_2, CO, and CH_4 are the molar fractions of the combustible gas components in the syngas, whereas $\dot{V_{gas}}$ (Nm^3/h) is the gas flow rate and $\dot{m_B}$ (kg/h) is the biomass consumption rate. It can be observed from Fig. 9 that the increase of the SBR leads to a decrease in the LHV, and consequently in the CGE and this tendency has been reported before in the study of Chutichai et al. [79]. Despite the increase in H_2, and CH_4, the drop in CO is comparatively significant, and this is the main reason for the drop in the LHV. Also, when the SBR is higher than 0.8, and since the hydrogen content starts to flip down, the decrease in the CGE intensifies and drops to 60% at the SBR of 1.4. Therefore, for the gasifier under investigation, and given that the goal of the study is to optimize the H_2 yield, the selected operating condition of the air/steam gasification is taken as 0.8, and this value is slightly lower than the values reported in some of the literature [75,80].

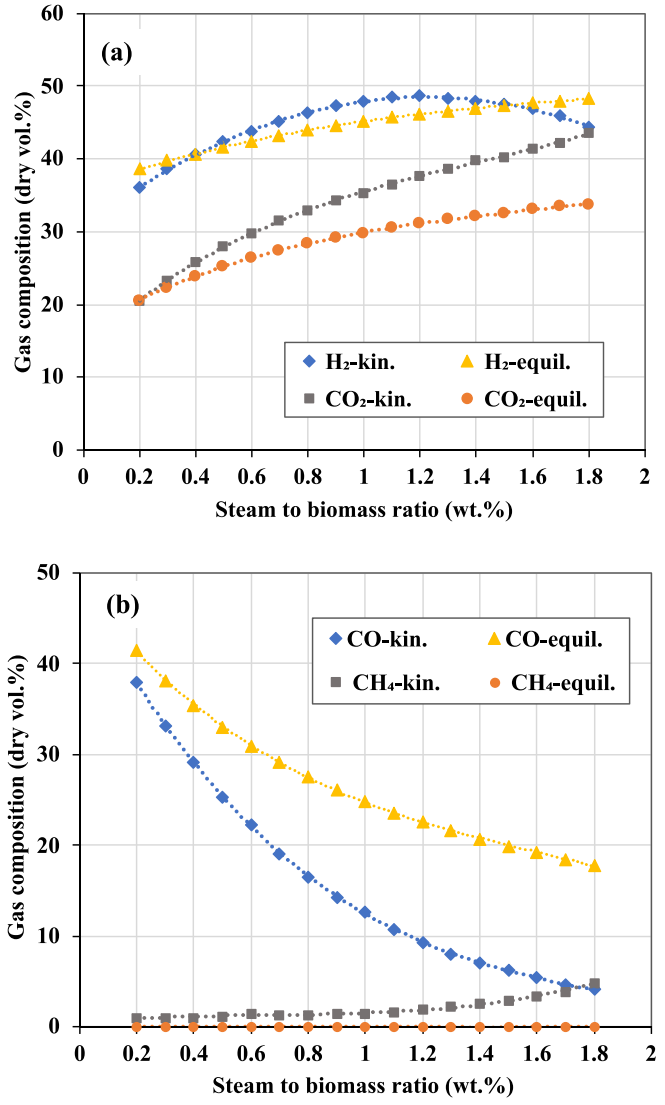

Fig. 10. Effect of SBR on the gas composition of the produced gas from the oxygen-based gasification process using the kinetic and the equilibrium models.

3.3.2. Steam-assisted oxygen gasification

The modelled gasifier has demonstrated its capability to operate efficiently with oxygen at an industrial scale and hence, this would be a more efficient approach for hydrogen production compared to air gasification. Consequently, it is essential to investigate the effect of steam addition to an oxy-gasifier system.

Fig. 10a shows that a similar trend to air–steam gasification is observed for the change in the H_2 content, where it increases from 36.0% to 48.6% as the SBR changes from 0.2 to 1.2. The increase in the hydrogen content under the oxy-steam gasification is even at a higher rate, where it increases by about 35.0% in comparison to 19.0% in the case of air–steam gasification (see Fig. 8). When the SBR exceeds 1.2, the hydrogen content starts to drop, and this is a similar behavior to the air–steam gasification but at higher values of SBR. This variation in the rate of change and in the sustained performance at higher SBR values is attributed to the operation with oxygen rather than air, in which the gasifier can still operate at higher temperatures even at higher SBRs.

Further, a comparison of the gas composition between the employed kinetic model and the equilibrium model is presented in Fig. 10, It can be observed that there is a noticeable difference between the models, where the equilibrium model shows different trends and different rates of change for the gas components. For example, the equilibrium model shows a continuous increase with an almost constant rate for the H_2 content (from 38.6% to 48.2%). This is a significant disadvantage of the equilibrium approach that can lead to overestimation of H_2 and inaccurate reactor designs. Also, the rate of reduction in the CO content, exhibited by the equilibrium model shown in Fig. 10, is less steep (from 41.4% to 17.8%) than the kinetic model, which decreases from 37.9% to 4.1% when the SBR changes from 0.2 to 1.8. These variations in the rates of change are mainly due to the consideration of the temperature change in the kinetic model in contrast to the equilibrium model.

Based on the predicted gas compositions, the effect of the SBR on the LHV and the CGE, following the kinetic and the equilibrium models, is presented in Fig. 11 and Fig. 12, respectively. When the SBR increases from 0.2 to 1.2 through the kinetic model, the LHV decreases from 9.1 MJ/m^3 to 7.0 MJ/m^3, while the CGE experiences only a slight decrease from 74.5% to 71.0%. This slight reduction in the CGE does not match the reduction rate in the LHV and this is due to the compensation caused by the increased gas yield in this range of SBRs [81]. However, the exact opposite behavior is noticed, where the LHV starts to plateau at around 7 MJ/m^3 and the CGE drops at higher rate from 71.0% to 62.6% when excess steam is added. Therefore, for the gasifier under investigation, the optimum operating condition for the steam-assisted oxygen gasification of wood chips is 1.2.

When it comes to the equilibrium-based gasification model, the effect of SBR on the LHV is less intense, where it drops from 9.3 MJ/m^3 to

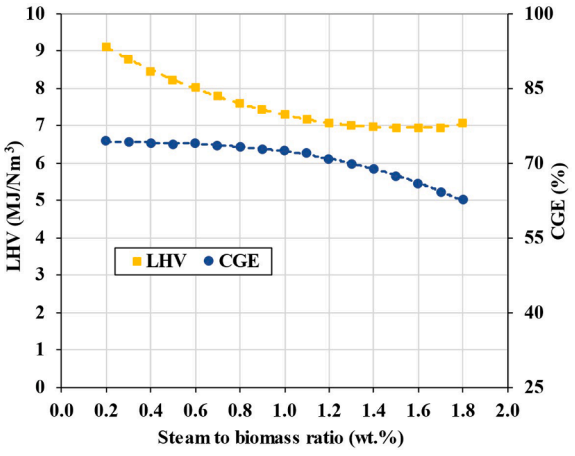

Fig. 11. Effect of the SBR on the gas LHV and the CGE of the process for the oxygen-based gasification process using the kinetic model.

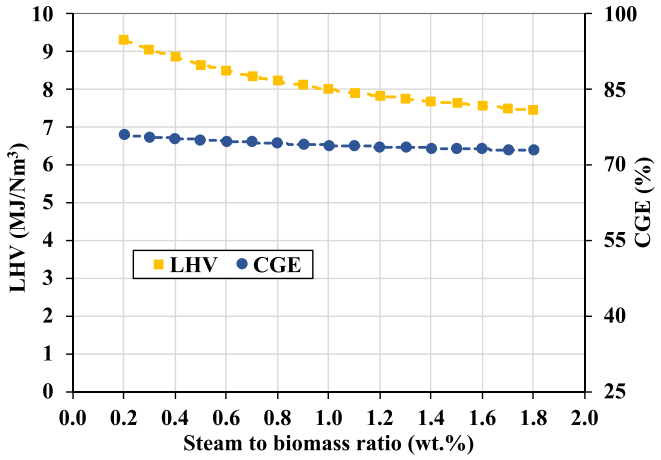

Fig. 12. Effect of the SBR on the gas LHV and the CGE of the process for the oxygen-based gasification process using the equilibrium model.

7.5 MJ/m^3 over the entire range of the studied SBRs (0.2–1.8). Also, the CGE exhibited a very slight change from 76.0% to 73.0% over the studied range of SBRs as presented in Fig. 12.

3.4. Sensitivity of the WGSRs towards the steam to CO ratio

An important parameter that affects the conversion of the CO in the syngas into H_2 and CO_2 through the WGS reaction is the steam to CO ratio (S/CO). Therefore, it is essential to perform a sensitivity analysis to identify the optimum performance of these reactors. The effect of the S/CO on the conversion of CO in the HTWGSR and the LTWGSR through the adopted kinetic model and an equilibrium-based model are shown in Fig. 13 and Fig. 14. The equilibrium-based model of the WGS reactors is built in Aspen Plus using the REquil reactors at 450 °C and 230 °C for the HTWGSR and the LTWGSR, respectively. It can be seen from Fig. 13 that the increase of the S/CO ratio increases the conversion of CO for both models; the rate of increase using the kinetic model is slower than the equilibrium one and the gap between the two models expands as the S/CO increases. By increasing the S/CO from 2 to 6, the conversion of CO can reach 36% for the kinetic, while it can go up to 60% for the equilibrium model.

After the HTWGSR, the gas is cooled down in order to reach the

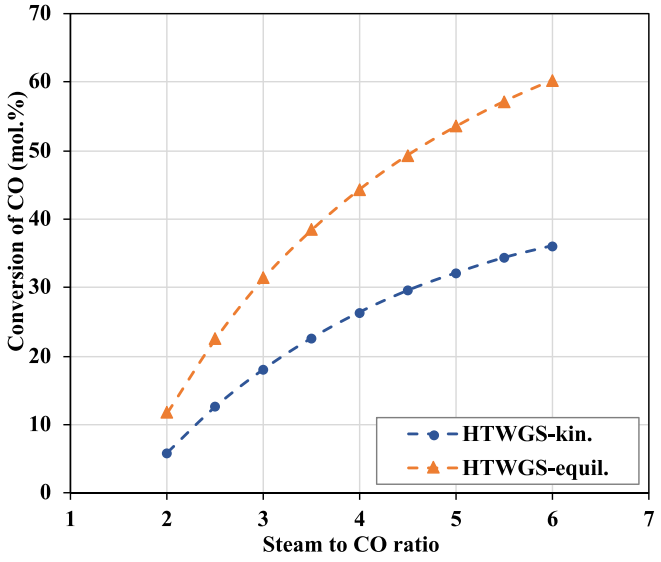

Fig. 13. Effect of the steam to CO ratio on the conversion of CO in the HTWGSR under the kinetic and the equilibrium models.

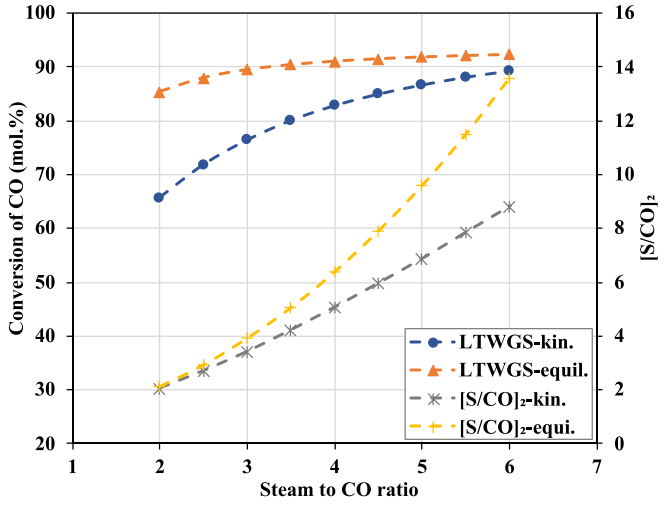

Fig. 14. Effect of the steam to CO ratio on the conversion of CO and on the intermediate S/CO prior to the LTWGSR under the kinetic and the equilibrium models.

operating temperature of the LTWGSR at 230 °C. The effect of the main S/CO on the conversion of CO in the LTWGSR and on the intermediate S/CO (i.e., the ratio before the LTWGSR, referred to as $[S/CO]_2$) is presented in Fig. 14. It can be noticed that $[S/CO]_2$ increases from both models with the increase of the main S/CO, where it starts almost at the same point at 2 and with the increase of S/CO up to 6, the $[S/CO]_2$ further increases and reaches 13.6 in the case of the equilibrium model and to 8.8% from the kinetic model. This is due to the high conversion of CO in the HTWGSR and since the WGS reaction consumes only one mole of H_2O per mole of CO (see equation (15), the extent of H_2O builds up as the conversion occurs. This high $[S/CO]_2$ boosts the WGS reaction even further until the equilibrium model becomes less dependent on the steam content. Whereas the kinetic model needs high S/CO to achieve a near-equilibrium conversion of CO, as can be seen in Fig. 14. Since the amount of steam required needs high energy to be supplied, a balanced choice should be made between the S/CO and the achieved conversion of CO. Hence, based on the available steam from the gasification process at SBR of 1.2, a ratio of S/CO up to 4.0 can be provided and it can achieve a considerable conversion of CO, as can be seen from Fig. 14.

3.5. Hydrogen buildup throughout the system

The hydrogen content in the gas stream evolves throughout the process, where the hydrogen sources are the biomass itself and the steam injected. Fig. 15 presents how the mole flow of hydrogen changes

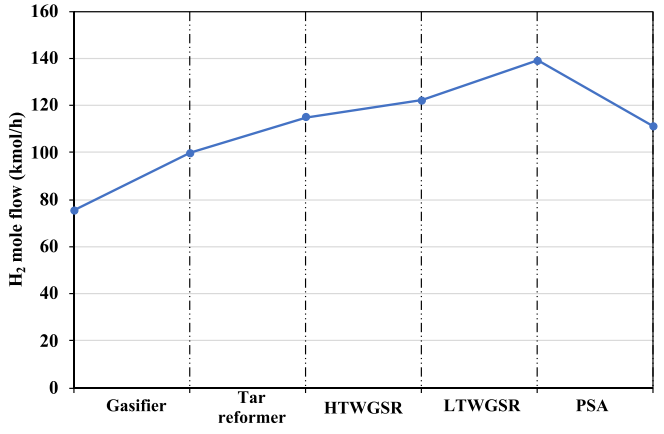

Fig. 15. Hydrogen buildup throughout the system components.

throughout the system. It can be noticed that the molar flow of hydrogen, which is originally impeded in the biomass at 75.4 kmol/h, substantially increases to 99.8 kmol/h during the gasification process. Following that, the rise in H_2 content persists through the tar reformer and the HTWGSR, where it reaches 122 kmol/h. This rate increases again as the temperature drops in the LTWGSR, which is in favor of the exothermic WGS reaction towards more conversion of CO. Finally, the obtained hydrogen flow from the PSA, at a recovery ratio of 80%, is 111.2 kmol/h. This represents a specific hydrogen yield of 81.5 gH_2/kg dry biomass. This is a little higher than the values reported in the literature at 80.4–64.0 gH_2/kg dry biomass [17,27,82]. For instance, the specific hydrogen yield has been reported as 64.0, 76.1, and 77.0 gH_2/kg of biomass from the systems based on DFB, BFB, and EF gasifiers, respectively [6,23]. Also, it is worth noting that, 27.8 kmol/h of hydrogen is left as part of the off gas, which is sent to the burner.

3.6. Energy distribution throughout the system

This section deals with the energy distribution throughout the system. It starts with the energy contained in the biomass and finishes with the final products i.e., H_2 and the liquid CO_2. Fig. 16 illustrates how the energy flows through the main system components, and it considers all the energy forms (i.e., the energy content in the material along with the sensible heat, and the electricity). With a biomass feeding rate of 2975 kg/h, the total energy flow to the system is 13.92 MW, which represents the driving power of the process. When the biomass is gasified, about 72% of the energy is converted into syngas (i.e., 9.99 MW), and 3.42 MW as a sensible heat in the gas steam. Then, when the syngas is reformed at an elevated temperature (900 °C) in the tar reformer with the heat supplied from the PSA off-gas burner, the energy content of the gas becomes 10.30 MW, while the sensible heat flow holds 2.69 MW after generating steam with a rate 1.80 MW. The sensible heat flow declines as the gas is cooled down to meet the operating temperature of the HTWGSR and the LTWGSR, where the syngas energy flow becomes 10.00 MW after the LTWGSR. Finally, the hydrogen can be acquired from the PSA at a rate of 224.19 kg/h, which is equivalent to an energy flow of 7.47 MW. Furthermore, Fig. 16 shows the electrical power needed for the system, mainly for the compression work in the PSA unit and for the capture and the storage of CO_2. The power needed for the PSA is 0.71 MW and for the CO_2 compression is 0.52 MW, and with the contribution from the ORC, i.e., 0.07 MW, the total electricity needed is 1.14 MW. Therefore, the overall energy efficiency of the system can be estimated as 49.6%, and this is higher than the efficiency of the entrained flow-based hydrogen production system, which is reported at 45.6% [17].

3.7. Carbon footprint

In order to evaluate the impact of such a system towards climate change, the carbon footprint of the process is assessed. The emission factors of the biomass feedstock and the electricity are considered as 16.60 $kgCO_2$-eq/MWh of fuel and 0.205 $kgCO_2$-eq/kWh, respectively. The biomass emission factor is based on the UK forest residues, where it includes the processing and transportation [83]. Also, the electricity emission factor is based on the UK grid mix [84]. The emission factor of oxygen is considered as 0.095 $kgCO_2/kgO_2$, which is obtained from SimaPro software based on the UK grid electricity. By assuming 8,000 h/year of operation for the system, the indirect CO_2-eq emissions due to upstream processing of biomass and the grid electricity used is 5,219.42 tCO_2-eq/year. Whereas the amount of CO_2 captured and stored is 38,145.04 tCO_2-eq/year, and hence the system is a negative emission and has the potential to permanently store a net of 36,107.28 tCO_2-eq/year. Consequently, the emission factor of the process is estimated at −1.38 $kgCO_2$-eq/kg biomass. To account for the uncertainties in the emission factors of the wood chips and the grid electricity, a sensitivity analysis has been carried out by assuming ± 100% variation to the adopted values. Accordingly, the emission factor of the system can vary between −1.25 and −1.50 $kgCO_2$-eq/kg biomass as can be seen in Fig. 17; this indicates that even at extreme pessimistic values for the grid electricity and feedstcok upstream emission factors, the proposed process is still net negative.

4. Conclusion

The current study provides, through comprehensive process modelling, the technical assessment of the biomass-based hydrogen production process from the two-stage industrial gasifier (NOTAR) at a capacity of 10 MW_{th} (of syngas). The modelling approach utilizes a reliable

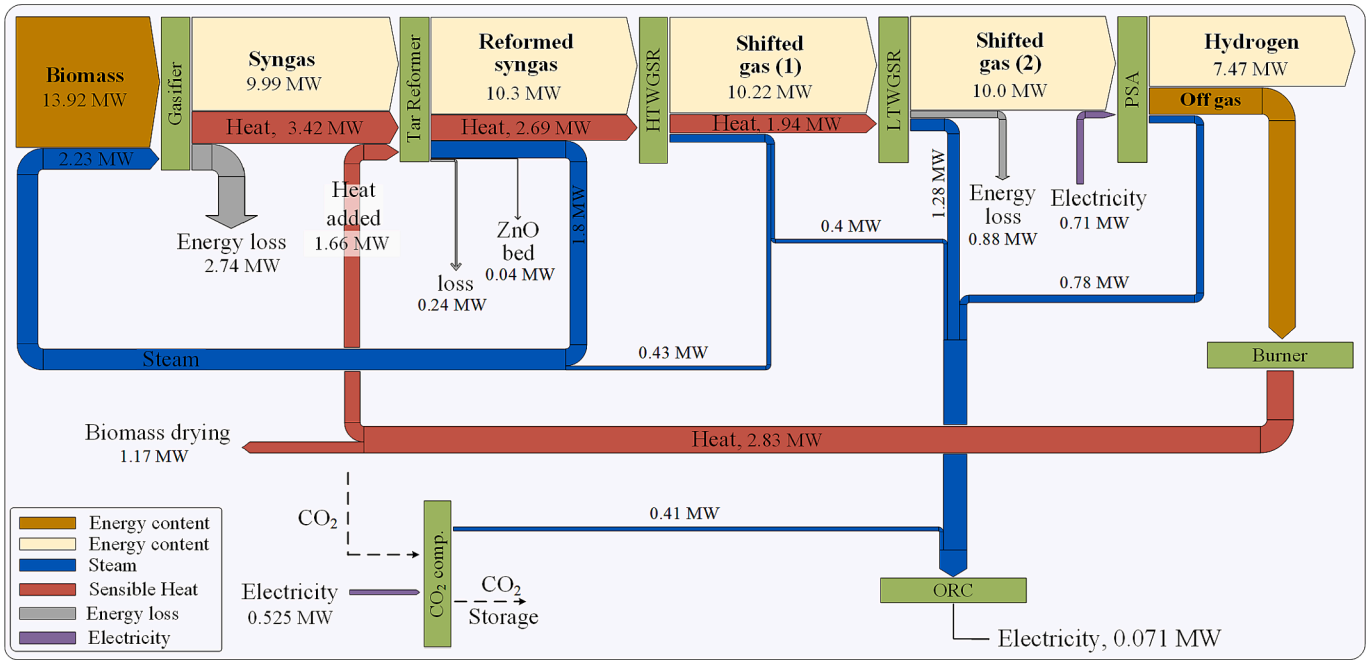

Fig. 16. Energy flow distribution throughout the system components.

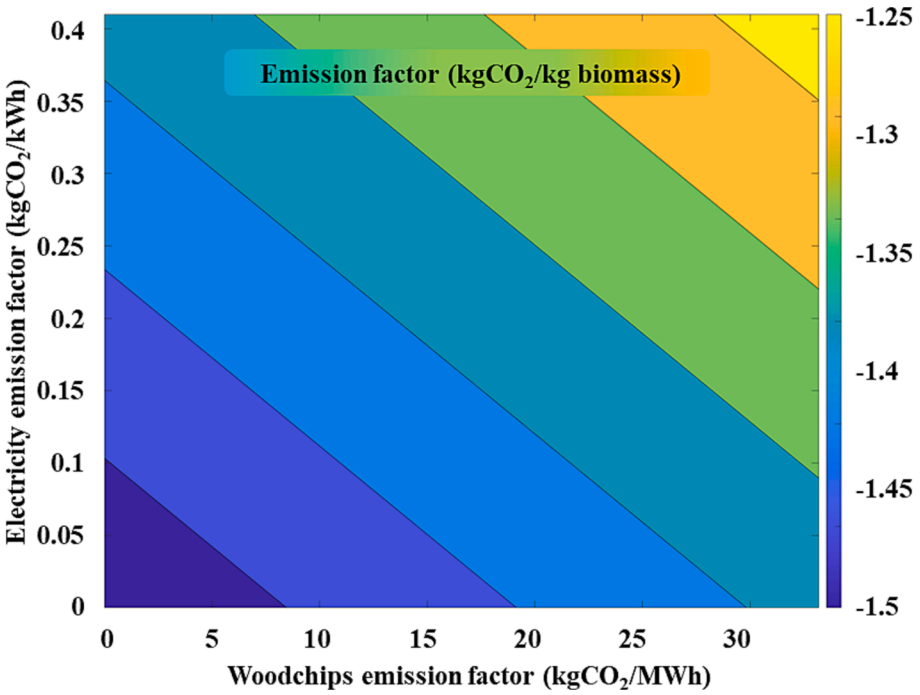

Fig. 17. Effect of the emission factors of the wood chips and grid electricity on the emission factor of the system.

kinetic model for the gasifier to simulate syngas production and to optimize the gasifier performance. Also, the study employs a kinetic reaction model for both WGSRs as a more realistic approach. The main outcomes of this study can be summarized as follows:

- The model has shown a high validity to simulate the two-stage gasifier at different scales (200 kW_{th} up to 1 MW_{th}) and under different operating conditions with a RMSD ranging from 0.529 vol% to 1.208 vol%, which represents a close agreement with the experimental data.
- By utilizing the validated model, the optimum gasifier performance for hydrogen production is investigated following air–steam and oxy-steam gasification. It has been revealed that the optimum SBR is 0.8 and 1.2 for the air–steam and oxy-steam gasification, respectively.
- Following the oxy-steam gasification at SBR of 1.2, the produced syngas is then upgraded through a tar reformer and two WGS reactors, where the LTWGS reaction is achieved at a S/CO of 4. This has achieved an overall CO conversion of 82.9%in both reactors.
- The model shows that the two-stage NOTAR gasifier can achieve a specific hydrogen yield of 81.47 gH_2/kg dry biomass. This is higher than the yield reported from other types of gasifiers, and this encourages the consideration of the two-stage gasifier for hydrogen production.
- The by-produced CO_2 is captured and compressed for storage at a rate of 4,768 kg/h, which makes the system a net negative emission technology. The emission factor of the investigated H_2 production process is −1.38 $kgCO_2$-eq/kg biomass.
- After an appropriate heat integration, the energy efficiency of biomass conversion to hydrogen is 49.6%.

This study is important as it presents reliable technical data for hydrogen production from biomass using the two-stage fixed bed gasifier and represents a solid foundation for economic and environmental studies. The configuration of the system through the developed flexible model can provide meaningful information to operating H_2-BECCS plants.

CRediT authorship contribution statement

Karim Rabea: Conceptualization, Formal analysis, Investigation, Methodology, Software, Validation, Writing – original draft. **Stavros Michailos:** Conceptualization, Methodology, Software, Validation, Writing – review & editing. **Kevin J. Hughes:** Resources, Supervision, Writing – review & editing. **Derek Ingham:** Project administration, Resources, Supervision, Writing – review & editing. **Mohamed Pourkashanian:** Resources, Supervision, Writing – review & editing.

Declaration of Competing Interest

The authors declare that they have no known competing financial interests or personal relationships that could have appeared to influence the work reported in this paper.

Data availability

Data will be made available on request.

Acknowledgement

The first author acknowledges The Egyptian Ministry of Higher Education & Scientific Research and The British Council (Newton-Mosharafa Fund) for funding this research study at the University of Sheffield.

Appendix A. Supplementary data

Supplementary data to this article can be found online at https://doi.org/10.1016/j.enconman.2023.117812.

References

[1] Singh V, Das D. Potential of hydrogen production from biomass. Sci Eng Hydrogen-based Energy Technol 2019:123–64.
[2] IEA, ''Global Hydrogen Review 2022''. 2022: Paris, https://www.iea.org/reports/global-hydrogen-review-2022.
[3] Shahbaz M, AlNouss A, Ghiat I, Mckay G, Mackey H, Elkhalifa S, et al. A comprehensive review of biomass based thermochemical conversion

technologies integrated with CO2 capture and utilisation within BECCS networks. Resour Conserv Recycl 2021;173:105734.
[4] Michaga MFR, Michailos S, Akram M, Cardozo E, Hughes KJ, Ingham D, et al. Bioenergy with carbon capture and storage (BECCS) potential in jet fuel production from forestry residues: A combined Techno-Economic and Life Cycle Assessment approach. Energ Conver Manage 2022;255:115346.
[5] Greencorn MJ, Jackson SD, Hargreaves JS, Datta S, Paul MC. Enhancement of gasification in oxyfuel BECCS cycles employing a direct recycling CO2 utilisation process. Energ Conver Manage 2023;277:116601.
[6] Salkuyeh YK, Saville BA, MacLean HL. Techno-economic analysis and life cycle assessment of hydrogen production from different biomass gasification processes. Int J Hydrogen Energy 2018;43(20):9514–28.
[7] Asadullah M. Biomass gasification gas cleaning for downstream applications: A comparative critical review. Renew Sustain Energy Rev 2014;40:118–32.
[8] Cheng F, Small AA, Colosi LM. The levelized cost of negative CO2 emissions from thermochemical conversion of biomass coupled with carbon capture and storage. Energ Conver Manage 2021;237:114115.
[9] Niu Y, Han F, Chen Y, Lyu Y, Wang L. Experimental study on steam gasification of pine particles for hydrogen-rich gas. J Energy Inst 2017;90(5):715–24.
[10] Song T, Wu J, Shen L, Xiao J. Experimental investigation on hydrogen production from biomass gasification in interconnected fluidized beds. Biomass Bioenergy 2012;36:258–67.
[11] Couto N, Rouboa A, Silva V, Monteiro E, Bouziane K. Influence of the biomass gasification processes on the final composition of syngas. Energy Procedia 2013;36:596–606.
[12] Kaydouh M-N, El Hassan N. Thermodynamic simulation of the co-gasification of biomass and plastic waste for hydrogen-rich syngas production. Results in Engineering 2022;16:100771.
[13] Mostafavi E, Mahinpey N, Rahman M, Sedghkerdar MH, Gupta R. High-purity hydrogen production from ash-free coal by catalytic steam gasification integrated with dry-sorption CO2 capture. Fuel 2016;178:272–82.
[14] Nam H, Wang S, Sanjeev K, Seo MW, Adhikari S, Shakya R, et al. Enriched hydrogen production over air and air-steam fluidized bed gasification in a bubbling fluidized bed reactor with CaO: Effects of biomass and bed material catalyst. Energ Conver Manage 2020;225:113408.
[15] Voldsund M, Jordal K, Anantharaman R. Hydrogen production with CO2 capture. Int J Hydrogen Energy 2016;41(9):4969–92.
[16] Habibi R, Mehrpooya M. A novel integrated Ca-Cu cycle with coal/biomass gasification unit for clean hydrogen production. Energ Conver Manage 2021;228:113682.
[17] Spath P, Aden A, Eggeman T, Ringer M, Wallace B, Jechura J. Biomass to hydrogen production detailed design and economics utilizing the Battelle Columbus Laboratory indirectly-heated gasifier. Golden, CO (US): National Renewable Energy Lab; 2005.
[18] Susmozas A, Iribarren D, Zapp P, Linβen J, Dufour J. Life-cycle performance of hydrogen production via indirect biomass gasification with CO2 capture. Int J Hydrogen Energy 2016;41(42):19484–91.
[19] Cohce M, Rosen M, Dincer I. Efficiency evaluation of a biomass gasification-based hydrogen production. Int J Hydrogen Energy 2011;36(17):11388–98.
[20] Antonini C, Treyer K, Moioli E, Bauer C, Schildhauer TJ, Mazzotti M. Hydrogen from wood gasification with CCS–a techno-environmental analysis of production and use as transport fuel. Sustain Energy Fuels 2021;5(10):2602–21.
[21] Michailos S, Emenike O, Ingham D, Hughes KJ, Pourkashanian M. Methane production via syngas fermentation within the bio-CCS concept: A techno-economic assessment. Biochem Eng J 2019;150:107290.
[22] Wu N, Lan K, Yao Y. An integrated techno-economic and environmental assessment for carbon capture in hydrogen production by biomass gasification. Resour Conserv Recycl 2023;188:106693.
[23] Ersöz A, DurakÇetin Y, Sarıoğlan A, Turan A, Mert M, Yüksel F, et al. Investigation of a novel & integrated simulation model for hydrogen production from lignocellulosic biomass. Int J Hydrogen Energy 2018;43(2):1081–93.
[24] Helf A, Cloete S, Keller F, Cloete JH, Zaabout A. Carbon-negative hydrogen from biomass using gas switching integrated gasification: Techno-economic assessment. Energ Conver Manage 2022;270:116248.
[25] Marcantonio V, De Falco M, Capocelli M, Bocci E, Colantoni A, Villarini M. Process analysis of hydrogen production from biomass gasification in fluidized bed reactor with different separation systems. Int J Hydrogen Energy 2019;44(21):10350–60.
[26] Kalinci Y, Hepbasli A, Dincer I. Exergoeconomic analysis and performance assessment of hydrogen and power production using different gasification systems. Fuel 2012;102:187–98.
[27] Martins AH, Rouboa A, Monteiro E. On the green hydrogen production through gasification processes: A techno-economic approach. J Clean Prod 2023;383:135476.
[28] Thomson R, Kwong P, Ahmad E, Nigam K. Clean syngas from small commercial biomass gasifiers; a review of gasifier development, recent advances and performance evaluation. Int J Hydrogen Energy 2020;45(41):21087–111.
[29] Xylowatt. ''NOTAR Gasifier''. 11/1/2023]; Available from: https://www.xylowatt.com/notar-gasifier/.
[30] Ferreira S, Monteiro E, Brito P, Vilarinho C. A holistic review on biomass gasification modified equilibrium models. Energies 2019;12(1):160.
[31] Berger B. Experimental and numerical investigation of a two-stage downdraft biomass gasification process. Belgium: Université catholique de Louvain Louvain-la-Neuve; 2018.
[32] Milhé M, Van de Steene L, Haube M, Commandre J-M, Fassinou W-F, Flamant G. Autothermal and allothermal pyrolysis in a continuous fixed bed reactor. J Anal Appl Pyrol 2013;103:102–11.
[33] Damon JP, Bacq A, Berger B, Dubois P, Bourgois F, Jeanmart H. Environmental benefits with used railway sleepers fueling Xylowatt's NOTAR Gasification technology. In: 20th European Biomass Conference and Exhibition; 2012.
[34] Xylowatt. ''The use of pure oxygen in a NOTAR® gasifier''. 2015 10/04/2023]; Available from: https://xylowatt.com/wp-content/uploads/2016/08/REGATEC-2015.pdf.
[35] Rabea K, Michailos S, Akram M, Hughes KJ, Ingham D, Pourkashanian M. An improved kinetic modelling of woody biomass gasification in a downdraft reactor based on the pyrolysis gas evolution. Energ Conver Manage 2022;258:115495.
[36] Qi J, Wang Y, Hu M, Xu P, Yuan H, Chen Y. A reactor network of biomass gasification process in an updraft gasifier based on the fully kinetic model. Energy 2023:126642.
[37] Tanoh TS, Oumeziane AA, Lemonon J, Escudero-Sanz FJ, Salvador S. A novel two-stage gasification strategy for nitrogen-free syngas production-pilot-scale experiments. Fuel Process Technol 2021;217:106821.
[38] Ghodke P, Mandapati RN. Investigation of particle level kinetic modeling for babul wood pyrolysis. Fuel 2019;236:1008–17.
[39] François J, Abdelouahed L, Mauviel G, Patisson F, Mirgaux O, Rogaume C, et al. Detailed process modeling of a wood gasification combined heat and power plant. Biomass Bioenergy 2013;51:68–82.
[40] Kumar M, Ghoniem AF. Multiphysics simulations of entrained flow gasification. Part II: Constructing and validating the overall model. Energy Fuel 2012;26(1):464–79.
[41] Wu Y, Zhang Q, Yang W, Blasiak W. Two-dimensional computational fluid dynamics simulation of biomass gasification in a downdraft fixed-bed gasifier with highly preheated air and steam. Energy Fuel 2013;27(6):3274–82.
[42] Salem AM, Paul MC. An integrated kinetic model for downdraft gasifier based on a novel approach that optimises the reduction zone of gasifier. Biomass Bioenergy 2018;109:172–81.
[43] Wang Y, Kinoshita C. Kinetic model of biomass gasification. Sol Energy 1993;51(1):19–25.
[44] Sharma AK. Modeling and simulation of a downdraft biomass gasifier 1. Model development and validation. Energ Conver Manage 2011;52(2):1386–96.
[45] Gómez-Barea A, Leckner B. Modeling of biomass gasification in fluidized bed. Prog Energy Combust Sci 2010;36(4):444–509.
[46] Robinson PJ, Luyben WL. Simple dynamic gasifier model that runs in Aspen Dynamics. Ind Eng Chem Res 2008;47(20):7784–92.
[47] Damartzis T, Michailos S, Zabaniotou A. Energetic assessment of a combined heat and power integrated biomass gasification–internal combustion engine system by using Aspen Plus®. Fuel Process Technol 2012;95:37–44.
[48] Beheshti S, Ghassemi H, Shahsavan-Markadeh R. Process simulation of biomass gasification in a bubbling fluidized bed reactor. Energ Conver Manage 2015;94:345–52.
[49] Umeki K, Yamamoto K, Namioka T, Yoshikawa K. High temperature steam-only gasification of woody biomass. Appl Energy 2010;87(3):791–8.
[50] Su Y, Luo Y, Chen Y, Wu W, Zhang Y. Experimental and numerical investigation of tar destruction under partial oxidation environment. Fuel Process Technol 2011;92(8):1513–24.
[51] Buentello-Montoya D, Zhang X, Marques S, Geron M. Investigation of competitive tar reforming using activated char as catalyst. Energy Procedia 2019;158:828–35.
[52] Mutlu ÖÇ, Zeng T. Challenges and Opportunities of Modeling Biomass Gasification in Aspen Plus: A Review. Chem Eng Technol 2020;43(9):1674–89.
[53] Lopez-Echeverry JS, Reif-Acherman S, Araujo-Lopez E. Peng-Robinson equation of state: 40 years through cubics. Fluid Phase Equilib 2017;447:39–71.
[54] Plus A. 1, Getting Started Modeling Processes with Solids. Cambridge, MA: Aspen Technology Inc; 2004.
[55] Singh M, Salaudeen SA, Gilroyed BH, Dutta A. Simulation of biomass-plastic co-gasification in a fluidized bed reactor using Aspen plus. Fuel 2022;319:123708.
[56] Diyoke C, Gao N, Aneke M, Wang M, Wu C. Modelling of down-draft gasification of biomass–An integrated pyrolysis, combustion and reduction process. Appl Therm Eng 2018;142:444–56.
[57] Ratnadhariya J, Channiwala S. Three zone equilibrium and kinetic free modeling of biomass gasifier–a novel approach. Renew Energy 2009;34(4):1050–8.
[58] Xylowatt. ''What is the power range of the installation ?''. 28/1/2023]; Available from: https://xylowatt.com/faq/.
[59] Park D, Duffy G, Edwards J, Roberts D, Ilyushechkin A, Morpeth L, et al. Kinetics of high-temperature water-gas shift reaction over two iron-based commercial catalysts using simulated coal-derived syngases. Chem Eng J 2009;146(1):148–54.
[60] Saw SZ, Nandong J. 'Simulation and control of water-gas shift packed bed reactor with inter-stage cooling. In IOP Conference Series: Materials Science and Engineering. IOP Publishing; 2016.
[61] Smith RJ B, Loganathan M, Shantha MS. A review of the water gas shift reaction kinetics. Int J Chem Reactor Eng 2010;8(1).
[62] Mendes D, Chibante VN, Mendes AL, Madeira LM. Determination of the low-temperature water– gas shift reaction kinetics using a Cu-based catalyst. Ind Eng Chem Res 2010;49(22):11269–79.
[63] Chen W-H, Chen C-Y. Water gas shift reaction for hydrogen production and carbon dioxide capture: A review. Appl Energy 2020;258:114078.
[64] Elliott WR. Front-End Engineering Design (FEED) Study for a Carbon Capture Plant Retrofit to a Natural Gas-Fired Gas Turbine Combined Cycle Power Plant (2x2x1 Duct-Fired 758-MWe Facility with F Class Turbines). Bechtel National, Inc., Reston, VA (United States); 2021.
[65] Han S, Seo J, Choi B-S. Development of a 200 kW ORC radial turbine for waste heat recovery. J Mech Sci Technol 2014;28:5231–41.

[66] Sung T, Yun E, Kim HD, Yoon SY, Choi BS, Kim K, et al. Performance characteristics of a 200-kW organic Rankine cycle system in a steel processing plant. Appl Energy 2016;183:623–35.
[67] Ozdil NFT, Segmen MR, Tantekin A. Thermodynamic analysis of an Organic Rankine Cycle (ORC) based on industrial data. Appl Therm Eng 2015;91:43–52.
[68] Tan Z, Feng X, Yang M, Wang Y. Energy and economic performance comparison of heat pump and power cycle in low grade waste heat recovery. Energy 2022;260:125149.
[69] Fu B-R, Lee Y-R, Hsieh J-C. Design, construction, and preliminary results of a 250-kW organic Rankine cycle system. Appl Therm Eng 2015;80:339–46.
[70] Kombe EY, Lang'at N, Njogu P, Malessa R, Weber C-T, Njoka F, et al. Process modeling and evaluation of optimal operating conditions for production of hydrogen-rich syngas from air gasification of rice husks using aspen plus and response surface methodology. Bioresour Technol 2022;361:127734.
[71] Tauqir W, Zubair M, Nazir H. Parametric analysis of a steady state equilibrium-based biomass gasification model for syngas and biochar production and heat generation. Energ Conver Manage 2019;199:111954.
[72] Basu P. Biomass gasification, pyrolysis and torrefaction: practical design and theory. Academic Press; 2018.
[73] Ong Z, Cheng Y, Maneerung T, Yao Z, Tong YW, Wang CH, et al. Co-gasification of woody biomass and sewage sludge in a fixed-bed downdraft gasifier. AIChE J 2015;61(8):2508–21.
[74] Narvaez I, Orio A, Aznar MP, Corella J. Biomass gasification with air in an atmospheric bubbling fluidized bed. Effect of six operational variables on the quality of the produced raw gas. Ind Eng Chem Res 1996;35(7):2110–20.
[75] Sharma S, Sheth PN. Air–steam biomass gasification: experiments, modeling and simulation. Energ Conver Manage 2016;110:307–18.
[76] Yan L, Lim CJ, Yue G, He B, Grace JR. One-dimensional modeling of a dual fluidized bed for biomass steam gasification. Energ Conver Manage 2016;127:612–22.
[77] Striūgas N, Zakarauskas K, Džiugys A, Navakas R, Paulauskas R. An evaluation of performance of automatically operated multi-fuel downdraft gasifier for energy production. Appl Therm Eng 2014;73(1):1151–9.
[78] Guo F, Dong Y, Dong L, Guo C. Effect of design and operating parameters on the gasification process of biomass in a downdraft fixed bed: An experimental study. Int J Hydrogen Energy 2014;39(11):5625–33.
[79] Chutichai B, Patcharavorachot Y, Assabumrungrat S, Arpornwichanop A. Parametric analysis of a circulating fluidized bed biomass gasifier for hydrogen production. Energy 2015;82:406–13.
[80] Nakyai T, Authayanun S, Patcharavorachot Y, Arpornwichanop A, Assabumrungrat S, Saebea D. Exergoeconomics of hydrogen production from biomass air-steam gasification with methane co-feeding. Energ Conver Manage 2017;140:228–39.
[81] Nguyen NM, Alobaid F, May J, Peters J, Epple B. Experimental study on steam gasification of torrefied woodchips in a bubbling fluidized bed reactor. Energy 2020;202:117744.
[82] Demol R, Dufour A, Rogaume Y, Mauviel G. Production of Purified H2, Heat, and Biochar from Wood: Comparison between Gasification and Autothermal Pyrolysis Based on Advanced Process Modeling. Energy Fuel 2021;36(1):488–501.
[83] Bates J, Henry S. Carbon factor for wood fuels for the Supplier Obligation; 2011, https://www.gov.uk/government/publications/carbon-factor-for-wood-fuels-for-the-supplier-obligation.
[84] Zero DfESN. 'Greenhouse gas reporting: conversion factors 2023; 2023, https://www.gov.uk/government/publications/greenhouse-gas-reporting-conversion-factors-2023.